Performance Limits of Optical Clock Recovery Systems Based on Two-Photon Absorption Detection Scheme

Hadi Zarkoob and Jawad A. Salehi, *Senior Member, IEEE*

***Abstract*—In this paper, we analyze and discuss the performance limits of optical clock recovery systems using a phase-locked loop (PLL) structure with nonlinear two-photon absorption (TPA) phase detection scheme. The motivation in analyzing the aforementioned optical PLL with TPA receiver structure is due to a recent successful experiment reported in [8]. We characterize the mathematical structure of PLLs with TPA, so as to evaluate the performance limits on optical clock recovery mechanism. More specifically, we identify two intrinsic sources of phase noise in the system namely, the ON–OFF nature of the incoming data pulses and the detector's shot noise that ultimately limit the performance of the aforementioned optical clock recovery system. In our characterization of the clock recovery system, we obtain the power spectral densities (PSDs) of the signals involved in the PLL and use the PSDs to obtain a mathematical expression for the variance of the timing jitter inherently associated with the recovered clock. We examine the variance of the introduced timing jitter as a function of different system parameters such as power, bit rate, and pulsewidth of the data and clock signals. An interesting result is that the duty cycle factor near 4 in return to zero optical pulses is optimal in the sense that it minimizes the variance of the system phase noise.**

***Index Terms*—Optical clock recovery, optical phase-locked loops (OPLLs), performance limits, shot noise process, timing jitter in optical systems, two-photon absorption (TPA).**

I. Introduction

A CRITICAL section of almost all communication receivers is the process of clock recovery in order to synchronize the transmitter and receivers pairs. Recently, performing the process of clock recovery in optical domain has received much attention in order to overcome the speed limitations imposed by the electronic counterparts. The ultimate success in establishing optical networking for future communication need is to introduce all-optical signal processing using advanced and enabling technologies such as nonlinear devices in optical networks. Among optical nonlinear phenomena, the process of two-photon absorption (TPA) is a strong candidate for optical signal processing applications, as it is simple, inexpensive, and ultrafast. This technique is used for a variety of applications in optical communications including autocorrelation evaluation of narrow pulses [1], detection of the spectrally encoded optical code division multiple access (OCDMA) [2]–[5], optical sampling [6]–[8], and demultiplexing [9]. In particular, because of its quadratic nonlinearity, the process of TPA can be used to measure the correlation between two high-speed optical signals. Based on this feature, an optical clock recovery scheme for optical time-division multiplexed (OTDM) networks has been recently proposed that incorporates the process of TPA as the phase detection mechanism in a phase-locked loop (PLL) structure [8]. This system is shown to be polarization insensitive, broadband, low jitter, and scalable to high data rates. The operational principles of this PLL have been discussed in [8]; however, the values for the timing jitter associated with the recovered clock are reported based on experimental measurements. The aim of this paper is to characterize the mathematical structure of this PLL such that it will result in obtaining the variance of the timing jitter due to two intrinsic sources of phase noise in the system namely the ON–OFF nature of the incoming data and the detector's shot noise. This, in fact, determines the performance limits expected from such optical clock recovery scheme.

The rest of this paper is organized as follows. In Section II, we introduce the clock recovery system under consideration in this paper. Section III discusses the statistical model of the output signal from TPA. In particular, we discuss the statistical behavior of the cross-correlation function between the data and clock signals. In Section IV, we focus on the PLL error signal and obtain an analytical expression for the variance of timing jitter in the system. In Section V, we present and discuss numerical results, and in Section VI, we conclude the paper.

II. System Description

Fig. 1(a) shows a simplified diagram of the proposed PLL system. As depicted, high-speed optical data and clock signals are combined and focused onto the surface of a silicon avalanche photodiode. At wavelengths ranging from 1100 to 2200 nm, the effect of single photon absorption is negligible for silicon photodiode, because at these wavelengths, the energy of one incident photon is less than the bandgap energy of silicon [10], [11]. Nevertheless, simultaneous absorption of two incident photons provides enough energy for generating an electron-hole pair [1]. As a result, if the wavelengths of the impinging fields lie near 1550 nm, as is the case with this system, the dominant process in producing the output photocurrent will be due to TPA. By choosing the polarization state of the clock to be circular, it can be shown that the output photocurrent $i(t)$ obtained in this way

Manuscript received November 2, 2007; revised December 17, 2007. This work was supported in part by the Hi-Tech Industries Center and Iran National Science Foundation (INSF).

The authors are with the Optical Networks Research Laboratory (ONRL), Department of Electrical Engineering, Sharif University of Technology, 11365-9363 Tehran, Iran (e-mail: hadi@ee.sharif.edu; jasalehi@sharif.edu).

Color versions of one or more of the figures in this paper are available online at http://ieeexplore.ieee.org.

Digital Object Identifier 10.1109/JSTQE.2008.918666

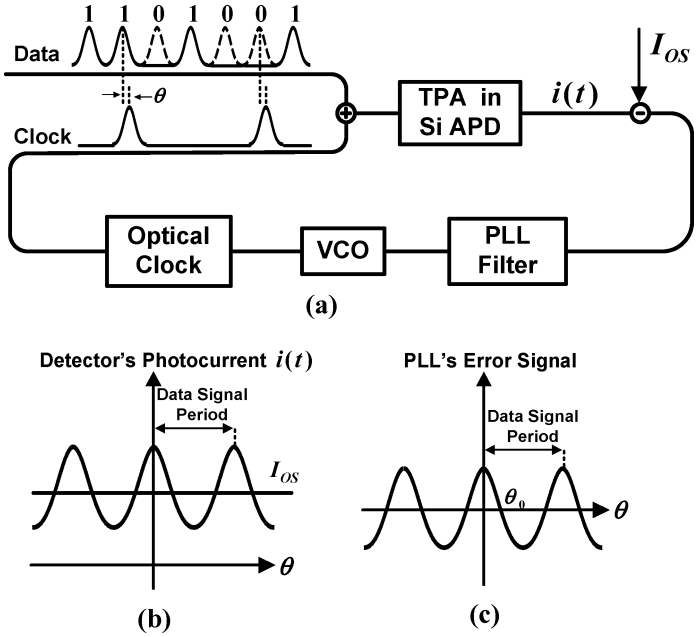

Fig. 1. (a) Optical clock recovery system representation. (b) TPA's photocurent as a function of the time delay between the clock and data signals θ. (c) PLL error signal.

is proportional to [8]

$$i(t) \propto \left(2\left\langle p_c^2(t-\theta)\right\rangle_t + \alpha\left\langle p_d^2(t)\right\rangle_t + 8\left\langle p_d(t)p_c(t-\theta)\right\rangle_t\right) \tag{1}$$

where $p_c(t)$ and $p_d(t)$ are power envelopes of the optical clock and data signals, respectively, and θ denotes the relative time delay between these two signals. The term α is a polarization-dependant factor whose value ranges from 2 to 3 depending on the degree of ellipticity of the data signal polarization state. In this equation, $\langle\cdot\rangle_t$ indicates the time average imposed by the detector's electron response. The first two terms in (1) are the time average of the data and clock signals and represent a constant background signal level. However, the third term is the cross-correlation between these two signals and directly depends on their relative time delay θ, as shown in Fig. 1(b). After subtracting a dc offset, denoted by $I_{\rm OS}$, the resulting bipolar signal is used as the error signal of the PLL. The feedback mechanism is designed in such a way that forces the error signal to zero, which then locks the clock and data signals together with a timing difference θ_0, determined by the position of the zero crossing point, as illustrated in Fig. 1(c).

There are several sources of phase noise that contribute to the timing jitter of the recovered clock in this system. The voltage-controlled oscillator (VCO) phase noise and the timing jitter of the incoming data pulses are just two examples. However, we do not consider them in this paper, as their behavior is identical in all PLLs and have been extensively examined in the literature [12]–[14]. In this paper, in particular, we consider the effect of two other sources of timing jitter that are intrinsic to such optical clock recovery systems and cannot be reduced by using lower noise electronic devices. The first source of noise considered is due to the fact that it is a random sequence of ON or OFF pulses that interacts with the clock signal in order to produce the error signal, leading to some random fluctuations in the resulting error signal. The second source of noise is the shot noise of the detector. Generally, the shot noise at the output of a photodiode is small when compared to the mean of the output photocurrent. However, in this optical clock recovery system, we subtract the constant offset $I_{\rm OS}$ from the detector's output photocurrent, hence, forcing it to fluctuate around zero. By doing so, we reduce the SNR at the output of the photodetector and bring out the effect of the shot noise in the system.

III. Statistical Modeling

In our statistical modeling of the aforementioned sources of noise, we begin by noting that the output photocurrent from the detector, i.e., $i(t)$, is a *filtered shot noise process* [15]. And the intermediate nonfiltered shot noise process, denoted by $a(t)$, is generated by the input count rate process $n(t)$, expressed as

$$\eta(t) = \eta\left(2p_c^2(t-\theta) + \alpha p_d^2(t) + 8p_d(t)p_c(t-\theta)\right) \tag{2}$$

where η is an efficiency factor proportional to the TPA coefficient of the detector. The actual detector's photocurrent, i.e., $i(t)$, is produced by passing $a(t)$ through a filter whose impulse response is the electron response of the detector, denoted as $h_e(t)$. The Fourier transform of $h_e(t)$, $H_e(f)$, has the attribute that $H_e(0) = q$, where q represents the elementary charge.

It can be easily shown that instead of subtracting the dc offset $I_{\rm OS}$ from the detector's actual photocurrent, we can subtract a dc amount of $A_{\rm OS} = I_{\rm OS}/H_e(0) = I_{\rm OS}/q$ from $a(t)$ prior to passing it through $h_e(t)$. In this way, we can combine $h_e(t)$ with the PLL filter and deal with $a(t)$ as the output of the photodiode, and hence, responsible for producing the PLL's error signal. The mean and power spectra of $a(t)$ are closely related to those of $n(t)$ as [15], [16]

$$\overline{a(t)} = \bar{g}\,\overline{n(t)} \tag{3}$$

$$S_{a,a}(f) = \overline{g^2}\,\overline{n(t)} + \bar{g}^2 S_{n,n}(f) \tag{4}$$

where the bar sign indicates statistical average and $S_{a,a}(f)$ and $S_{n,n}(f)$ represent the power spectral densities (PSDs) of $a(t)$ and $n(t)$, respectively. The terms $\bar{g}$ and $\overline{g^2}$ represent the first and the second moment of the detector's avalanche gain.

To obtain the statistical properties of $n(t)$, which is a prerequisite in obtaining the statistical properties of $a(t)$, we assume that the data and the clock signals are of the form

$$p_d(t) = \sum_{m=-\infty}^{+\infty} b_m \tilde{p}_d(t - mT_d) \tag{5}$$

$$p_c(t) = \sum_{m=-\infty}^{+\infty} \tilde{p}_c(t - mT_c) \tag{6}$$

where $b_m \in \{0, 1\}$ are data binary digits for ON–OFF keying modulation. The term θ is the time delay by which the clock signal follows the data signal. The terms T_d and T_c are the time durations of the data and clock pulses, respectively. In an OTDM network, assuming that there are N users in the network, we have $T_c = NT_d$. In (5) and (6), $\tilde{p}_d(t)$ and $\tilde{p}_c(t)$ denote zero-centered pulses of data and clock signals, respectively, and are assumed

to be Gaussian as

$$\tilde{p}_d(t) = 2P_d\sqrt{\frac{1}{\pi}}\frac{T_d}{w}\exp\left(-\frac{t^2}{w^2}\right)\prod_{T_d}(t)$$
$$= a_d\exp\left(-\frac{t^2}{w^2}\right)\prod_{T_d}(t) \quad (7)$$
$$\tilde{p}_c(t) = P_c\sqrt{\frac{1}{\pi}}\frac{T_c}{w}\exp\left(-\frac{t^2}{w^2}\right)\prod_{T_c}(t)$$
$$= a_c\exp\left(-\frac{t^2}{w^2}\right)\prod_{T_c}(t) \quad (8)$$

where P_d and P_c represent the average power of data and clock signals, w denotes the pulsewidth parameter, which, for simplicity, is assumed to be the same for both signals, and $\prod_T(t)$ denotes a zero-centered rectangular pulse with unit height and duration $T, T \in \{T_d, T_c\}$. Parameters $a_d = 2P_d\sqrt{(1/\pi)}(T_d/w)$ and $a_c = P_c\sqrt{(1/\pi)}(T_c/w)$ are simplified notations in representing the Gaussian pulse amplitudes. The factor 2 in $\tilde{p}_d(t)$ is due to the fact that the data signal is assumed to be comprised of equally likely ones and zeros. Using (5)–(8) in (2), we obtain

$$n(t) = \eta\left(2x(t-\theta) + \alpha y(t) + 8\left(\mathrm{z}_1\left(t-\frac{\theta}{2}\right) + \mathrm{z}_2\left(t-\frac{T_d+\theta}{2}\right)\right)\right) \quad (9)$$

where $x(t)$, $y(t)$, $z_1(t)$, and $z_2(t)$ are four auxiliary signals that are temporally aligned with $p_d(t)$, and are defined as

$$x(t) = \sum_{m=-\infty}^{+\infty}\tilde{x}(t-mT_c) \quad (10)$$
$$y(t) = \sum_{m=-\infty}^{+\infty}b_m\,\tilde{y}(t-mT_d) \quad (11)$$
$$z_1(t) = \sum_{m=-\infty}^{+\infty}b_{mN}\,\tilde{z}_1(t-mT_c) \quad (12)$$
$$z_2(t) = \sum_{m=-\infty}^{+\infty}b_{mN+1}\,\tilde{z}_2(t-mT_c) \quad (13)$$

where $\tilde{x}(t), \tilde{y}(t), \tilde{z}_1(t)$, and $\tilde{z}_2(t)$ are single zero-centered pulses given by

$$\tilde{x}(t) = a_c^2\exp\left(\frac{-2t^2}{w^2}\right)\prod_{T_c}(t) \quad (14)$$
$$\tilde{y}(t) = a_d^2\exp\left(\frac{-2t^2}{w^2}\right)\prod_{T_d}(t) \quad (15)$$
$$\tilde{z}_1(t) = a_d a_c\exp\left(\frac{-\theta^2}{2w^2}\right)\exp\left(\frac{-2t^2}{w^2}\right)\prod_{T_c}(t) \quad (16)$$
$$\tilde{z}_2(t) = a_d a_c\exp\left(\frac{-(T_d-\theta)^2}{2w^2}\right)\exp\left(\frac{-2t^2}{w^2}\right)\prod_{T_c}(t). \quad (17)$$

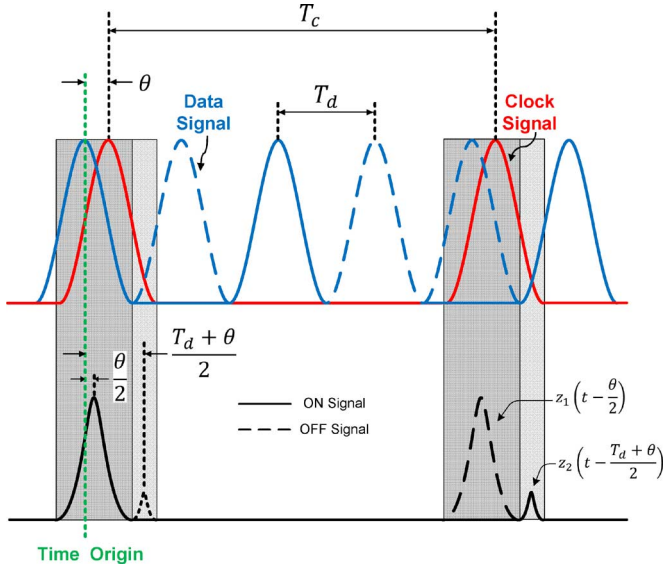

Fig. 2. Representation of $p_d(t)p_c(t-\theta)$ by the means of two auxiliary signals $z_1(t-\theta/2)$ and $z_2(t-(T_d+\theta)/2)$. Each clock pulse is assumed to have an overlap with at most two pulses of the data signal at each time.

In writing $p_d(t)p_c(t-\theta)$ as the sum of two signals $z_1\,(t-\theta/2)$ and $z_2\,(t-(T_d+\theta)/2)$, we have multiplied the mth pulse of the clock signal, i.e., $\tilde{p}_c(t-mT_c-\theta)$, by two consecutive pulses, i.e., $\tilde{p}_d(t-mNT_d)$ and $\tilde{p}_d(t-(mN+1)T_d)$, of the data signal for all integer values of m, as depicted in Fig. 2. In doing so, we have assumed that each clock pulse has an overlap with at most two pulses of the data signal at each time, which is a reasonable assumption when the pulsewidths of data and clock signals are not significantly different.

As the first step in considering the statistical properties of $n(t)$, we obtain the statistical mean of $n(t)$, conditioned on a fixed time difference of θ $(0 \le \theta \le T_d)$ between the data and the clock signals. All the auxiliary signals presented in (9) are cyclostationary processes. As a result, by assigning a common random phase with a uniform distribution between 0 and T_c to the signals $p_d(t)$ and $p_c(t)$ (which does not affect their relative time delay), we can find time-independent means of the aforementioned auxiliary signals in terms of their time average over one whole period. This random phase can be simply interpreted as the randomness existing in the time when the system is turned on and the signals are generated. Using the time-independent means of the aforementioned auxiliary signals, we can express the time-independent mean value of (3), denoted by $\bar{a}$, as

$$\overline{a(t)} = \bar{a} = \bar{g}\overline{n(t)}$$
$$= \bar{g}\eta\left(2P_c^2\frac{1}{\sqrt{2\pi}}\frac{T_c}{w} + \alpha P_d^2\sqrt{\frac{2}{\pi}}\frac{T_d}{w} + 8P_dP_c\frac{1}{\sqrt{2\pi}}\frac{T_d}{w}\left(\exp\left(\frac{-\theta^2}{2w^2}\right) + \exp\left(\frac{-(T_d-\theta)^2}{2w^2}\right)\right)\right). \quad (18)$$

IV. PLL Error Signal

In this section, we analyze and discuss the PLL error signal. It can be seen that the θ-dependant mean of $a(t)$ in (18) resembles the shape of the detector's photocurrent as a function of θ for $0 \leq \theta \leq T_d$, presented in Fig. 1(b). As previously mentioned, we reduce the value of $a(t)$ by the dc term $A_{\rm OS}$ to produce the PLL bipolar error signal in our model. However, this error signal, i.e., $a(t) - A_{\rm OS}$, is *degraded* due to random fluctuations of $a(t)$ around its mean $\bar{a}$. In fact, if we write $a(t)$ as the summation of its mean $\bar{a}$ and a zero-mean signal $n_a(t)$, then $n_a(t)$ plays the role of an additive noise term to the PLL's error signal. Assuming that the value of $\bar{a} - A_{\rm OS}$ is a linear function of θ in the vicinity of zero crossing point θ_0 [14], we can express the PLL error signal as

$$\begin{aligned} a(t) - A_{\rm os} &= (\bar{a} - A_{\rm os}) + n_a(t) = K_s(\theta - \theta_0) + n_a(t) \\ &= K_s\left(\theta + \frac{n_a(t)}{K_s} - \theta_0\right) = K_s(\theta + n_a'(t) - \theta_0) \end{aligned} \tag{19}$$

where K_s is the slope of $\bar{a}$ at $\theta = \theta_0$ and $n_a'(t) = n_a(t)/K_s$ is an equivalent noise term. The value of K_s can be obtained by evaluating the derivative of the third term in (18) with respect to θ at $\theta = \theta_0$; hence,

$$\begin{aligned} K_s = \bar{g}\eta\Bigg(8P_dP_c\frac{1}{\sqrt{2\pi}}\frac{T_d}{w}\Bigg(-\frac{\theta_0}{w^2}\exp\left(-\frac{\theta_0^2}{2w^2}\right) \\ + \frac{(T_d-\theta_0)}{w^2}\exp\left(-\frac{(T_d-\theta_0)^2}{2w^2}\right)\Bigg)\Bigg). \end{aligned} \tag{20}$$

If we denote the phase of the data and the clock signals by θ_d and θ_c, respectively, we can use the notation of $\theta_d - \theta_c$ to represent the time delay between these two signals instead of θ. By substituting this notation in (19), we can indicate the so-called noisy error signal of the PLL as

$$\begin{aligned} a(t) - A_{\rm os} &= K_s(\theta + n_a'(t) - \theta_0) \\ &= K_s(\theta_d + n_a'(t) - (\theta_c + \theta_0)). \end{aligned} \tag{21}$$

Equation (21) is a basic equation as it helps to demonstrate the PLL in the *phase domain*. In the phase domain representation of the PLL, the phases of data and clock signals lie at the input and output terminals, respectively, and $n_a'(t)$ represents a noise term that is added to the input signal of the PLL. An illustration of the phase-domain representation of the PLL is presented in Fig. 3.

From Fig. 3, the closed-loop frequency response of the PLL at the phase domain, denoted by $G(f)$, can be expressed as

$$G(f) = \frac{K_sH_s(f)H_{\rm PLL}(f)H_{\rm VCO}(f)}{1 + K_sH_s(f)H_{\rm PLL}(f)H_{\rm VCO}(f)}. \tag{22}$$

Based on the phase-domain representation of the PLL, we can obtain the variance of the PLL's output timing jitter in terms of the PSD of $n_a'(t)$ and the PLL's closed-loop frequency response

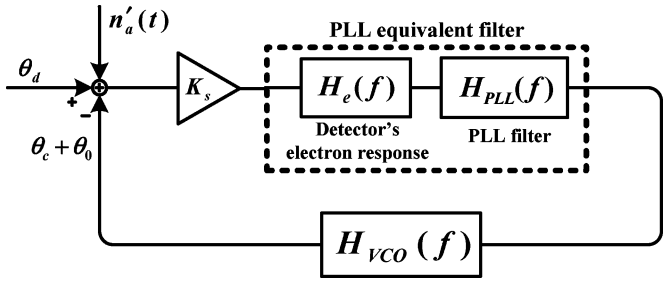

Fig. 3 PLL's phase-domain model.

$G(f)$ as

$$\begin{aligned} \sigma_p^2 &= \int_{-\infty}^{+\infty} S_{n_a',n_a'}(f)\,|G(f)|^2\,df \\ &= \int_{-\infty}^{+\infty} \frac{S_{n_a,n_a}(f)}{K_s^2}\,|G(f)|^2\,df \\ &= \frac{S_{n_a,n_a}(0)}{K_s^2}\int_{-\infty}^{+\infty}|G(f)|^2\,df = \frac{2S_{n_a,n_a}(0)B_f}{K_s^2} \end{aligned} \tag{23}$$

where B_f is (one sided) equivalent closed-loop bandwidth of the PLL, defined as

$$B_f = \int_0^{\infty}|G(f)|^2\,df. \tag{24}$$

The third equality in (23) arises from the fact that the closed-loop bandwidth of the PLL is much narrower compared to the optical broadband PSD of $n_a'(t)$.

From (23), to obtain the value of σ_p^2, we first obtain the value of $S_{n_a,n_a}(0)$. To do this, we evaluate the value of $S_{a,a}(f)$ at the dc frequency that differs from $S_{n_a,n_a}(0)$ by the expression $\bar{a}^2\delta(f)$, i.e., $S_{n_a,n_a}(0) = S_{a,a}(f)\,|_{\rm dc\,freq.} - \bar{a}^2\delta(f)$. Equation (4) indicates that $S_{a,a}(f)\,|_{\rm dc\,freq.}$ is comprised of two terms. The first term, denoted by $S_{\rm shot}$, is due to the shot noise and equals to

$$S_{\rm shot} = \overline{g^2}\bar{n} = F_A\bar{g}^2\bar{n} \tag{25}$$

where F_A is the excess noise factor of the avalanche photodiode and the value of $\bar{n}$ is implicitly given by (18). The second term of $S_{a,a}(f)\,|_{\rm dc\,freq.}$ is proportional to the PSD of $n(t)$ at the dc frequency. Using the representation given in (9), we can obtain the autocorrelation function of $n(t)$, and then, evaluate its Fourier transform $S_{n,n}(f)$ at the dc frequency. In the Appendix, it is shown that the resulting value for $S_{n,n}(f)$ at the dc frequency, after being multiplied by $\bar{g}^2$, is expressed as

$$\begin{aligned} \bar{g}^2S_{n,n}(f)\,|_{\rm dc\,freq.} &= \bar{a}^2\delta(f) + \bar{g}^2\eta^2\Bigg(\frac{\alpha^2\tilde{Y}^2(0)}{4T_d} \\ &+ \frac{16\big(\tilde{Z}_1^2(0) + \tilde{Z}_2^2(0)\big)}{T_c} + \frac{4\alpha\tilde{Y}(0)\big(\tilde{Z}_1(0) + \tilde{Z}_2(0)\big)}{T_c}\Bigg) \end{aligned} \tag{26}$$

where $\tilde{Y}(f)$, $\tilde{Z}_1(f)$, and $\tilde{Z}_2(f)$ denote the Gaussian Fourier transforms of the Gaussian-shaped pulses $\tilde{y}(t)$, $\tilde{z}_1(t)$, and $\tilde{z}_2(t)$, respectively. If we denote the second term in (26) by $S_{\rm bin}$,

the value of $S_{\rm bin}$ can be obtained by substituting the Fourier transforms presented in (26) by their value at $f = 0$, as

$$S_{\rm bin} = \bar{g}^2\eta^2 \left(\frac{2\alpha P_d^4 T_d^3}{\pi w^2} + \frac{32 P_d^2 P_c^2 T_d^2 T_c}{\pi w^2} \left(\exp\left(-\frac{\theta^2}{w^2}\right) + \exp\left(-\frac{(T_d-\theta)^2}{w^2}\right)\right) + \frac{16\alpha P_d^3 P_c T_d^3}{\pi w^2} \left(\exp\left(-\frac{\theta^2}{2w^2}\right) + \exp\left(-\frac{(T_d-\theta)^2}{2w^2}\right)\right)\right). \quad (27)$$

Based on the parameters $S_{\rm shot}$ and $S_{\rm bin}$ and using (4), the value of $S_{n_a,n_a}(0)$ can be obtained as

$$S_{n_a,n_a}(0) = S_{a,a}(f)|_{\rm dc\ freq.} - \bar{a}^2\delta(f) = \overline{g^2}\bar{n} + \bar{g}^2 S_{n,n}(f)\,|_{\rm dc\ freq.} - \bar{a}^2\delta(f) = S_{\rm shot} + S_{\rm bin} \quad (28)$$

where in writing the last equality, we have used the definitions of the parameters $S_{\rm shot}$ and $S_{\rm bin}$ presented earlier. Substituting the value of $S_{n_a,n_a}(0)$ from (28) in (23), we obtain

$$\sigma_p^2 = \frac{S_{n_a,n_a}(0)B_f}{K_s^2} = \frac{S_{\rm shot}B_f}{K_s^2} + \frac{S_{\rm bin}B_f}{K_s^2} = \sigma_{\rm shot}^2 + \sigma_{\rm bin}^2 \quad (29)$$

where $\sigma_{\rm shot}^2$ and $\sigma_{\rm bin}^2$ correspond to terms including $S_{\rm shot}$ and $S_{\rm bin}$, respectively. Equation (29) indicates that the variance of the timing jitter inherently associated with the recovered clock is represented as the sum of two terms corresponding to the two intrinsic sources of phase noise introduced in Section II.

Note that the value of $S_{n_a,n_a}(0)$ (and thus σ_p^2) is a function of θ (due to the θ-dependence of both $S_{\rm shot}$ and $S_{\rm bin}$ terms), and consequently, it would be hard to analyze the system for arbitrary changes of θ. However, when the PLL reaches its steady state, the value of θ changes only over a small interval around θ_0 denoted by $(\theta_0 - d\theta, \theta_0 + d\theta)$. It can be seen that, for practical values of $d\theta$, the value of $S_{n_a,n_a}(0)$ changes only slightly over this interval, and as a result, in obtaining the value of $S_{n_a,n_a}(0)$, we can use the value of θ_0 as a representative of the whole interval $(\theta_0 - d\theta, \theta_0 + d\theta)$. In the next section, we will use a set of practical values for the system parameters to obtain the value of $S_{n_a,n_a}(0)$ for different values of θ and numerically demonstrate this feature.

V. Numerical Results

In this section, we numerically investigate the analytical results presented in the previous section. We begin by giving a numerical example using the same system parameters reported in the experiment in [8], namely, $P_d = 6$ mW, $P_c = 12$ mW (which corresponds to average powers of 3 and 6 mW for data and clock signals, respectively, in the passband), $T_d = 12.5$ ps, $T_c = 100$ ps, pulsewidth of data and clock signals [full-width at half-maximum (FWHM)] $= 4$ ps, $B_f = 5.5$ kHz. For parameter α, we use the representative value of 3 that corresponds to a linear polarization state for the data signal. The value of $\eta\bar{g}$ is estimated from the data given in [8] to be $\eta\bar{g} = 1.56 \times 10^{15}\ {\rm s}^{-1}{\rm W}^{-2}$. Finally, we substitute the following

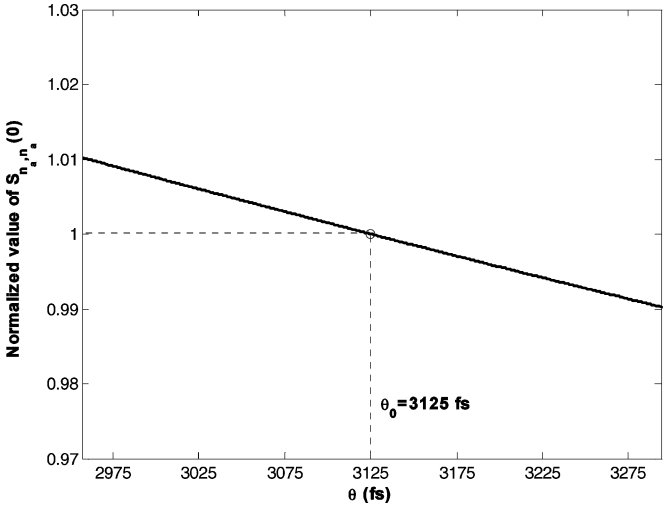

Fig. 4. Normalized value of $S_{n_a n_a}(0)$ versus the time delay between data and clock signals θ.

unknown variables by their typical values: $\bar{g} = 150$, $F_A = 5$ [17], [18], and $\theta_0 = T_d/4 = 3.125$ ps.

Employing these system parameters and using the value of θ_0 for θ, we obtain a theoretical value of $6.633 \times 10^{15}\ {\rm s}^{-1}$ for $S_{n_a,n_a}(0)$, resulting in a timing jitter of about $\sigma_p = 20$ fs. To examine the behavior of $S_{n_a,n_a}(0)$ in the vicinity of θ_0, we normalized this parameter by its value at $\theta = \theta_0$ and plot its normalized values as a function of θ in the neighborhood of θ_0, as depicted in Fig. 4. As illustrated, $S_{n_a,n_a}(0)$ deviates only by 1% of its value at $\theta = \theta_0$ for deviations of θ as large as 170 fs. This exceeds the practical values of the timing jitter associated with the recovered clock even at the presence of all experimental sources of timing jitter in the system. This, in fact, confirms the assumption that we can use the value of $S_{n_a,n_a}(0)$, obtained for $\theta = \theta_0$, in evaluating the value of σ_p in the system.

The value of 20 fs calculated here for σ_p, in comparison with the 110 fs timing jitter experimentally reported in [8], indicates that the timing jitter of the recovered clock in this system is mostly dominated by the electrical sources of the phase noise such as the noise due to VCO and the RF synthesizer at the receiver and transmitter sides, respectively. On the other hand, it indicates that by using lower noise system structures, the variance of the timing jitter associated with the recovered clock can be further improved and get close to the fundamental intrinsic limit, as obtained in this paper (see, e.g., [19]).

In Figs. 5–7, we investigate how the different system parameters such as power of the optical data and clock signals, number of users in the OTDM network and the data bit rate affect the value of σ_p. In plotting these figures, we use the aforementioned values as the default value of system parameters, and in each case, we vary the value of those parameters whose effect is under consideration. In the cases that we change the value of the data signal power to explore its effect, we simultaneously change the value of the clock signal power so that the ratio between these two quantities remains at 2. This is because a ratio of 2 between the power of the data and clock signals assures proper operation of the system for different polarization states of the input data

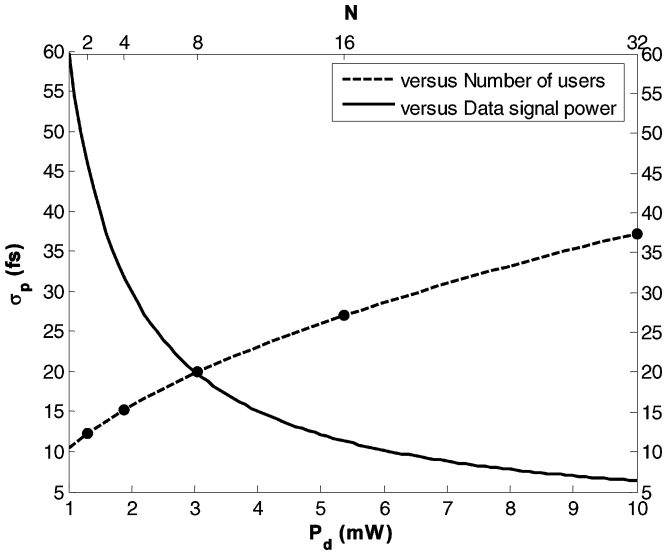

Fig. 5. Standard deviation of the inherent jitter in the system σ_p versus number of users in the OTDM network N and the data signal power P_d.

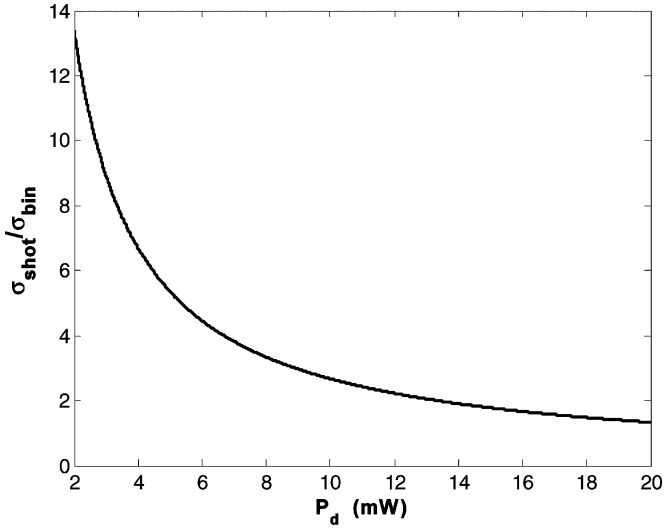

Fig. 6. Ratio between timing jitter due to two intrinsic sources of phase noise in the system versus the data signal power P_d.

signal [8]. Moreover, when we vary the duration of data pulses T_d to examine the effect of data bit rate, we concurrently change the duration of the clock pulses T_c and also the pulsewidth of both signals, so that the ratio between these parameters remains constant. This, indeed, helps us to deal with realistic parameters for data and clock signals.

Fig. 5 plots the value of σ_p as a function of the data signal power P_d and the number of users in the OTDM network N, using solid and dashed curves, respectively. As illustrated in the bottom axis, higher values for the signal powers lead to lower values for the variance of the intrinsic timing jitter in the system.

As previously mentioned, in an OTDM network, for a constant value of the data signal period T_d, the clock signal period T_c is determined by the number of users in the network N. In plotting the dashed curve in Fig. 5, we fix the parameter

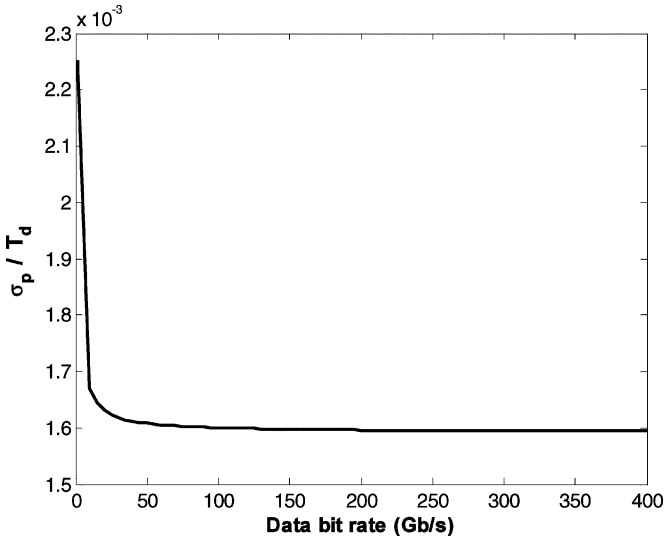

Fig. 7. Value of σ_p normalized by the data bit duration T_d versus data bit rate.

T_d and display the parameter σ_p as a function of the number of users in the network. The diagram for the values of $N = 2,\ 4,\ 8,\ 16,$ and 32 is marked by small circles. As depicted, the value of σ_p rises as the number of users increase in the network, which, in fact, is as a result of the corresponding increase in the value of T_c in the system.

To explore how the two introduced sources of phase noise contribute to the overall timing jitter of the system, we find it useful to plot the value of $\sigma_{\rm shot}/\sigma_{\rm bin}$ as a function of P_d, as depicted in Fig. 6. As illustrated, for lower values of P_d, it is the shot noise source that dominates the value of the inherent timing jitter in the system. However, at higher values of the signal powers, the contribution of $\sigma_{\rm bin}$ increases in the system and as a result, the value of σ_p is determined by the influence of both $\sigma_{\rm shot}$ and $\sigma_{\rm bin}$.

In Fig. 7, we examine the inherent timing jitter associated with the recovered clock for different values of the data bit rate. Since the duration of the data pulses T_d varies for different values of data bit rate, we plot the normalized value of σ_p, i.e., σ_p/T_d, as a function of the data bit rate. As illustrated in Fig. 7, the quantity σ_p/T_d demonstrates a sharp fall at lower values of data bit rate. However, it is relatively stabilized for data bit rates more than 100 Gb/s. It means that at lower values of bit duration, the value of timing jitter decreases so that the ratio σ_p/T_d remains approximately constant.

Finally, we study the dependence of σ_p on the pulsewidth parameter w of the signals (which is assumed to be the same for both data and clock pulses). To better investigate this dependence, we examine the value of σ_p as a function of the duty cycle factor f_p, defined as

$$f_p = \frac{T_d}{T_{\rm FWHM}} \tag{30}$$

where $T_{\rm FWHM}$ denotes FWHM of the data and clock pulses, and is closely related to the pulsewidth parameter w by the relation $T_{\rm FWHM} = 2\sqrt{\ln(2)}w$. In plotting Fig. 8, we display the value of σ_p as a function of f_p while keeping the parameter

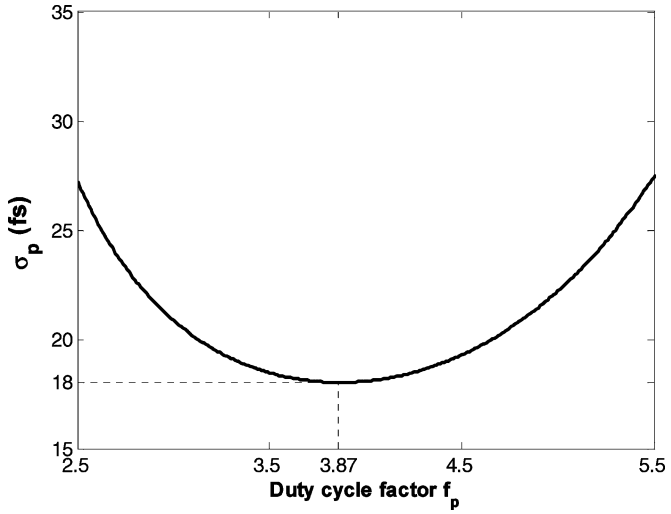

Fig. 8. Standard deviation of the inherent timing jitter in the system σ_p versus duty cycle factor of the data and clock pulses f_p.

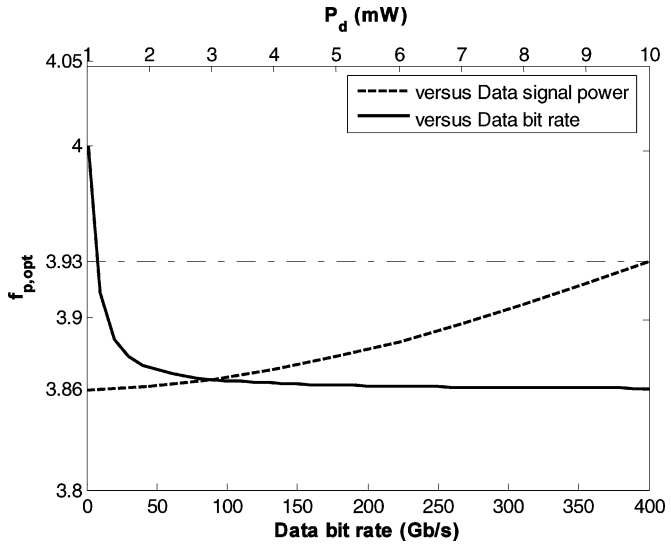

Fig. 9. Optimum duty cycle factor $f_{p,\mathrm{opt}}$ as a function of the data signal power P_d and the data bit rate.

T_d at a constant value. As illustrated in this figure, there is an optimum value for f_p, denoted by $f_{p,\mathrm{opt}}$, for which the value of σ_p is minimized. The value of $f_{p,\mathrm{opt}}$ for the system parameters described above turns out to be 3.87.

The existence of an optimum value for f_p can be explained by considering how (18) and (27) depend on w [(18) and (27) correspond to the shot noise source and binary data source, respectively]. For example, from (18), it follows that the cross-correlation between data and clock signals has a Gaussian pulse shape whose pulsewidth is proportional to w, while its amplitude inversely depends on w that leads to an interaction between two differently behaving (one decreasing and the other increasing) functions of w. Similar interactions occurs in (27) and their net effect determines the value of $f_{p,\mathrm{opt}}$.

It can be seen that the value of $f_{p,\mathrm{opt}}$ does not change considerably for a large range of system parameters. To illustrate this feature, we plot the value of $f_{p,\mathrm{opt}}$ as a function of the data bit rate and the data signal power in Fig. 9. As depicted, for a large variety of system parameters, the value of $f_{p,\mathrm{opt}}$ ranges only from 3.86 to 4. This leads us to the result that a duty cycle factor of about 4 can be regarded as optimal in this optical clock recovery system.

VI. Conclusion

In this paper, we analyzed, mathematically, a newly proposed optical clock recovery system based on TPA detection mechanism. We evaluated the effect of two intrinsic sources of timing jitter inherently limiting the performance of this system, namely, random nature of the incoming data pulses and the detector's shot noise. Based on the PSDs of the signals involved in the system, we obtained an analytical expression for the variance of the timing jitter intrinsically accompanying the recovered clock. We observed that the variance of the introduced timing jitter is inversely related to the input signal powers and the input data bit rate. However, its value rises as the number of users increases in an OTDM network. An interesting result was that, for a large variety of system parameters, a duty cycle factor of about 4 was shown to be optimal in the sense that it minimizes the variance of the timing jitter in the recovered clock.

Appendix

In the Appendix, we express the autocorrelation function of $n(t)$, denoted by $R_{n,n}(\tau)$, in order to obtain its Fourier transform at the dc frequency, i.e., $S_{n,n}(0)$. The value of $n(t)$ from (9) is given by

$$n(t) = \eta\left(2x(t-\theta) + \alpha y(t) + 8\left(z_1\left(t - \frac{\theta}{2}\right) + z_2\left(t - \frac{T_d+\theta}{2}\right)\right)\right). \tag{A1}$$

In obtaining the value of $R_{n,n}(\tau)$, as we described when presenting (18) of the paper, we assume a common random phase with uniform distribution over $(0, T_c)$ for all terms in (A1) which, as previously discussed, does not affect the validity of the results. At this step, we neglect the oscillations of θ in (A1) and obtain the autocorrelation function of $n(t)$ conditioned on a fixed θ. The value of $R_{n,n}(\tau)$ can be expressed in terms of the auto- and cross-correlation functions of its components presented in (A1) as

$$\begin{aligned} R_{n,n}(\tau) = {} & 4R_{x,x}(\tau) + \alpha^2 R_{y,y}(\tau) + 64R_{z_1,z_1}(\tau) \\ & + 64R_{z_2,z_2}(\tau) + 2\alpha\left(R_{x,y}(\tau-\theta) + R_{y,x}(\tau+\theta)\right) \\ & + 16\left(R_{x,z_1}\left(\tau - \frac{\theta}{2}\right) + R_{z_1,x}\left(\tau + \frac{\theta}{2}\right)\right) \\ & + 16\left(R_{x,z_2}\left(\tau + \frac{T_d-\theta}{2}\right)\right. \\ & \left. + R_{z_2,x}\left(\tau - \frac{T_d-\theta}{2}\right)\right) \end{aligned}$$

$$+8\alpha\left(R_{y,z_1}\left(\tau+\frac{\theta}{2}\right)+R_{z_1,y}\left(\tau-\frac{\theta}{2}\right)\right)$$
$$+8\alpha\left(R_{y,z_2}\left(\tau+\frac{T_d+\theta}{2}\right)\right.$$
$$\left.+R_{z_2,y}\left(\tau-\frac{T_d+\theta}{2}\right)\right)$$
$$+64\left(R_{z_1,z_2}\left(\tau+\frac{T_d}{2}\right)+R_{z_2,z_1}\left(\tau-\frac{T_d}{2}\right)\right). \tag{A2}$$

All of the auto- and cross-correlations presented in (A2) can be obtained using elementary stochastic processes theory and we list only the results

$$R_{x,x}(\tau)=\frac{1}{T_c}\tilde{x}(\tau)\circledast\tilde{x}(\tau) \tag{A3}$$

where the $\circledast$ sign shows the circular convolution operation between two pulses. The circular convolution operation between two arbitrary pulses $\tilde{w}_1(t)$ and $\tilde{w}_2(t)$ with durations T_1 and T_2, respectively, is defined in terms of the ordinary convolution operation between the first pulse and the periodically repeated version of the second pulse, as

$$\tilde{w}_1(t)\circledast\tilde{w}_2(t)=\tilde{w}_1(t)*\left(\sum_{m=-\infty}^{+\infty}\tilde{w}_2(t-mT_2)\right) \tag{A4}$$

where * denotes the ordinary convolution operation. Note that by this definition, the circular convolution operation is not a commutative operation when T_1 and T_2 are not identical.

For other correlation functions, we have

$$R_{y,y}(\tau)=\frac{1}{4T_d}\tilde{y}(\tau)\circledast\tilde{y}(\tau)+\frac{1}{4T_d}\tilde{y}(\tau)*\tilde{y}(\tau) \tag{A5}$$

$$R_{z_1,z_1}(\tau)=\frac{1}{4T_c}\tilde{z}_1(\tau)\circledast\tilde{z}_1(\tau)+\frac{1}{4T_c}\tilde{z}_1(\tau)*\tilde{z}_1(\tau) \tag{A6}$$

$$R_{z_2,z_2}(\tau)=\frac{1}{4T_c}\tilde{z}_2(\tau)\circledast\tilde{z}_2(\tau)+\frac{1}{4T_c}\tilde{z}_2(\tau)*\tilde{z}_2(\tau) \tag{A7}$$

$$R_{x,y}(\tau)=R_{y,x}(\tau)=\frac{1}{2T_d}\tilde{x}(\tau)\circledast\tilde{y}(\tau) \tag{A8}$$

$$R_{x,z_1}(\tau)=R_{z_1,x}(\tau)=\frac{1}{2T_c}\tilde{x}(\tau)\circledast\tilde{z}_1(\tau) \tag{A9}$$

$$R_{x,z_2}(\tau)=R_{z_2,x}(\tau)=\frac{1}{2T_c}\tilde{x}(\tau)\circledast\tilde{z}_2(\tau) \tag{A10}$$

$$R_{y,z_1}(\tau)=R_{z_1,y}(\tau)=\frac{1}{4T_c}\tilde{z}_1(\tau)\circledast\tilde{y}(\tau)+\frac{1}{4T_c}\tilde{z}_1(\tau)*\tilde{y}(\tau). \tag{A11}$$

The cross-correlation function between signals $z_2(t)$ and $y(t)$ can be obtained using a shifted version of $y(t)$ defined as $y'(t)=y(t+T_d)$. For $y'(t)$ defined in this way, it can be easily seen that the pulses of $z_2(t)$ are temporarily aligned with those pulses of $y'(t)$ that have contributed in constructing them. It can be shown that the cross-correlation function between signals $z_2(t)$ and $y(t)$ reads

$$R_{y',z_2}(\tau)=R_{z_2,y'}(\tau)=\frac{1}{4T_c}\tilde{z}_2(\tau)\circledast\tilde{y}(\tau)+\frac{1}{4T_c}\tilde{z}_2(\tau)*\tilde{y}(\tau). \tag{A12}$$

Since $y'(t)$ is a shifted version of $y(t)$, the values of $R_{y,z_2}(\tau)$ and $R_{z_2,y}(\tau)$ can be directly obtain from $R_{y',z_2}(\tau)$ and $R_{z_2,y'}(\tau)$ as

$$R_{y,z_2}(\tau)=R_{y',z_2}(\tau-T_d) \tag{A13}$$

$$R_{z_2,y}(\tau)=R_{z_2,y'}(\tau+T_d). \tag{A14}$$

And finally, we have

$$R_{z_1,z_2}(\tau)=R_{z_2,z_1}(\tau)=\frac{1}{4T_c}\tilde{z}_1(\tau)\circledast\tilde{z}_2(\tau). \tag{A15}$$

Using (A3) and (A5)–(A15) in (A2) gives us the value of $R_{n,n}(\tau)$. The Fourier transform of $R_{n,n}(\tau)$, i.e., $S_{n,n}(f)$, can be obtained using elementary properties of the Fourier transform. The resulting value of $S_{n,n}(f)$ at the dc frequency would be

$$S_{n,n}(f)\,|_{\mathrm{dc\,freq.}}=\bar{n}^2\delta(f)$$
$$+\eta^2\left(\frac{\alpha^2\tilde{Y}^2(0)}{4T_d}+\frac{16\big(\tilde{Z}_1^2(0)+\tilde{Z}_2^2(0)\big)}{T_c}\right.$$
$$\left.+\frac{4\alpha\tilde{Y}(0)\big(\tilde{Z}_1(0)+\tilde{Z}_2(0)\big)}{T_c}\right). \tag{A16}$$

Multiplying both sides of (A16) by $\bar{g}^2$, leads us to the (26) of the paper.

REFERENCES

[1] F. R. Laughton, J. H. Marsh, D. A. Barrow, and E. L. Portnoi, "The two-photon absorption semiconductor waveguide autocorrelator," *IEEE J. Quantum Electron.*, vol. 30, no. 3, pp. 838–845, Mar. 1994.

[2] Z. Zheng, A. M. Weiner, J. H. Marsh, and M. M. Karkhanehchi, "Ultrafast optical thresholding based on two-photon absorption GaAs waveguide photodetectors," *IEEE Photon. Technol. Lett.*, vol. 9, no. 4, pp. 493–495, Apr. 1997.

[3] Z. Zheng, H. Sardesai, C. C. Chang, S. Shen, A. M. Weiner, J. H. Marsh, and M. M. Kharkhanehchi, "Nonlinear detection of spectrally coded ultrashort pulse by two-photon absorption GaAs waveguide photodetectors," in *Proc. Conf. Lasers Electro-Opt. (CLEO)*, San Francisco, CA, 1998, pp. 97–98.

[4] K. Jamshidi and J. A. Salehi, "Performance analysis of spectral-phase-encoded optical CDMA system using two-photon-absorption receiver structure for asynchronous and slot-level synchronous transmitters," *J. Lightw. Technol.*, vol. 25, no. 6, pp. 1638–1645, Jun. 2007.

[5] K. Jamshidi and J. A. Salehi, "Statistical characterization and bit-error rate analysis of lightwave systems with optical amplification using two-photon-absorption receiver structures," *J. Lightw. Technol.*, vol. 24, no. 3, pp. 1302–1316, Mar. 2006.

[6] K. Kikuchi, "Optical sampling system at 1.5 mm using two photon absorption in Si avalanche photodiode," *Electron. Lett.*, vol. 34, no. 13, pp. 1354–1355, Jun. 1998.

[7] P. J. Maguire, L. P. Barry, T. Krug, M. Lynch, A. L. Bradley, J. F. Donegan, and H. Folliot, "All-optical sampling utilizing two-photon absorption in semiconductor microcavity," *Electron. Lett.*, vol. 41, no. 8, pp. 489–490, Apr. 2005.

[8] R. Salem, A. A. Ahmadi, G. E. Tudury, G. M. Carter, and T. E. Murphy, "Two-photon absorption for optical clock recovery in OTDM networks," *J. Lightw. Technol.*, vol. 24, no. 9, pp. 3353–3362, Sep. 2006.

[9] B. C. Thomsen, L. P. Barry, J. M. Dudley, and J. D. Harvey, "Ultrahigh speed all-optical demultiplexing based on two-photon absorption in a laser diode," *Electron. Lett.*, vol. 34, no. 19, pp. 1871–1872, Sep. 1998.

[10] H. Folliot, M. Lynch, A. L. Bradley, T. Krug, L. A. Dunbar, J. Hegarty, J. F. Dunegan, and L. P. Barry, "Two-photon-induced photoconductivity enhancement in semiconductor microcavities: A theoretical investigation," *J. Opt. Soc. Amer. B, Opt. Phys.*, vol. 19, no. 10, pp. 2396–2402, Oct. 2002.
[11] M. Sheik-Bahae, D. C. Hutchkins, D. J. Hagan, and E. W. Van Stryland, "Dispersion of bound electronic nonlinear refraction in solids," *IEEE J. Quantum Electron.*, vol. 27, no. 6, pp. 1296–1309, Jun. 1991.
[12] A. J. Viterbi, *Principles of Coherent Communication*. New York: McGraw-Hill, 1966.
[13] F. M. Gardner, *Phaselock Techniques*. New York: Wiley, 1979.
[14] R. E. Best, *Phase-locked Loops: Design, Simulation and Applications*. New York: McGraw-Hill, 2003.
[15] R. M. Gagliardi and S. Karp, *Optical Communications*. New York: Wiley, 1995, ch. 3.
[16] D. L. Snyder and M. I. Miller, *Random Point Processes in Time and Space*. New York: Springer-Verlag, 1991.
[17] S. D. Cova, A. L. Lacaita, L. Andrea, F. Zappa, and P. G. Lovati, "Avalanche photodiodes for near infrared photon-counting," *Proc. SPIE*, vol. 2388, pp. 56–66, 1995.
[18] H. Dautet, P. Deschamps, B. Dion, A. D. MacGregor, D. MacSween, R. J. McIntyre, C. Trottier, and P. P. Webb, "Photon counting techniques with silicon avalanche photodiodes," *Appl. Opt.*, vol. 32, no. 21, pp. 3894–3900, Jul. 1993.
[19] S. Takasaka, Y. Ozeki, and M. Sakano, "Synchronization of a 160-GHz optical beat signal with a 2-ps optical RZ signal by phase-locked loop technique," in *Proc. Optical Fiber Commun. Conf. (OFC 2007)*, Mar. 2007, Anaheim, CA, Paper OME6.

Hadi Zarkoob was born in Isfahan, Iran, on June 24, 1983. He received the B.S. and M.S. degrees (with honors) in electrical engineering from Sharif University of Technology (SUT), Tehran, in 2005 and 2007, respectively.

Since 2008, he has been a member of the Optical Network Research Laboratory (ONRL), Sharif University of Technology. His current research interests include mathematical modeling and statistical characterization of optical communications systems.

Jawad A. Salehi (M'84–SM'07) was born in Kazemain, Iraq, on December 22, 1956. He received the B.S. degree from the University of California, Irvine, in 1979, and the M.S. and Ph.D. degrees from the University of Southern California (USC), Los Angeles, in 1980 and 1984, respectively, all in electrical engineering.

He is currently a Full Professor at the Optical Networks Research Laboratory (ONRL), Department of Electrical Engineering, Sharif University of Technology (SUT), Tehran, Iran, where he is also the Co-Founder of the Advanced Communications Research Institute (ACRI). From 1981 to 1984, he was a Full-Time Research Assistant at the Communication Science Institute, USC. From 1984 to 1993, he was a Member of Technical Staff of the Applied Research Area, Bell Communications Research (Bellcore), Morristown, NJ. During 1990, he was with the Laboratory of Information and Decision Systems, Massachusetts Institute of Technology (MIT), Cambridge, as a Visiting Research Scientist. From 1999 to 2001, he was the Head of the Mobile Communications Systems Group and the Co-Director of the Advanced and Wideband Code-Division Multiple Access (CDMA) Laboratory, Iran Telecom Research Center (ITRC), Tehran. From 2003 to 2006, he was the Director of the National Center of Excellence in Communications Science, Department of Electrical Engineering, SUT. He is the holder of 12 U.S. patents on optical CDMA. His current research interests include optical multiaccess networks, optical orthogonal codes (OOC), fiber-optic CDMA, femtosecond or ultrashort light pulse CDMA, spread-time CDMA, holographic CDMA, wireless indoor optical CDMA, all-optical synchronization, and applications of erbium-doped fiber amplifiers (EDFAs) in optical systems.

Prof. Salehi is an Associate Editor for Optical CDMA of the IEEE TRANSACTIONS ON COMMUNICATIONS since May 2001. In September 2005, he was elected as the Interim Chair of the IEEE Iran Section. He was the recipient of several awards including the Bellcore's Award of Excellence, the Nationwide Outstanding Research Award from the Ministry of Science, Research, and Technology in 2003, and the Nation's Highly Cited Researcher Award in 2004. He is among the 250 preeminent and most influential researchers worldwide in the *Institute for Scientific Information (ISI) Highly Cited in the Computer-Science Category*. He is the corecipient of the IEEE's Best Paper Award in 2004 from the International Symposium on Communications and Information Technology, Sapporo, Japan.